Molecular Crystals and Liquid Crystals
Publication details, including instructions for authors and subscription information:
http://www.tandfonline.com/loi/gmcl16

Thermodynamic Properties of Ferrocene-d_{10} Crystal: Comparison with Ferrocene-h_{10}

M. Soral [a] & Y. Shloml [a]
[a] Chemical Thermodynamics Laboratory. Faculty of Science, Osaka University, Toyonaka, Osaka, 560, Japan
Version of record first published: 20 Apr 2011.

To cite this article: M. Soral & Y. Shloml (1984): Thermodynamic Properties of Ferrocene-d_{10} Crystal: Comparison with Ferrocene-h_{10} , Molecular Crystals and Liquid Crystals, 107:3-4, 271-292

To link to this article: http://dx.doi.org/10.1080/00268948408070441

Mol. Cryst. Liq. Cryst., 1984, Vol. 107, pp. 271–292
0026-8941/84/1074–0271/$18.50/0

Printed in the United States of America

Thermodynamic Properties of Ferrocene-d_{10} Crystal: Comparison with Ferrocene-h_{10}†

M. SORAI and Y. SHIOMI

Chemical Thermodynamics Laboratory, Faculty of Science, Osaka University, Toyonaka, Osaka 560, Japan

(*Received September 23, 1983*)

The heat capacities of deuterated bis (η^5-cyclopentadienyl) iron [$Fe(C_5D_5)_2$: ferrocene-d_{10} for short] have been measured between 13 and 300 K with an adiabatic calorimeter. A λ-type phase transition centered at 164.1 K with a subsidiary small peak at 172 K was found between the metastable low-temperature (LT) phase and the undercooled high-temperature (HT) phase. The stable LT phase exhibited a first-order transition to the HT phase at 251 K. The enthalpy and entropy of both the transitions were essentially the same as those of ferrocene-h_{10} whereas the temperature of the first-order transition shifted 9 K in comparison with ferrocene-h_{10}. The heat capacity differences between ferrocene-d_{10} and -h_{10} for these three phases were well accounted for in terms of a change in the normal mode frequencies and the $(C_p - C_v)$ correction. As in the case of ferrocene-h_{10}, ferrocene-d_{10} crystals showed a violent disintegration phenomenon with vast evolution of heat below the λ-point.

1. INTRODUCTION

Recent reinvestigations of ferrocene-h_{10} crystal on the basis of calorimetry,[1-3] structural analyses[4-10] and spectroscopies[11,12] have disclosed new aspects of its physicochemical properties, in particular, the phase relationship including the stable low-temperature phase newly found and the molecular conformations and arrangements in each phase. However, the mechanism of the particular phase transitions has not been well understood. We thought that the isotope effect on the crystal behavior would give some clue to this problem. One of the

†Contribution No. 66 from Chemical Thermodynamics Laboratory.

objects of this paper is to report the results of heat capacity measurements on deuterated ferrocene (ferrocene-d_{10}) between 13 and 300 K, and to compare with those of ferrocene-h_{10}. A part of the results was briefly given previously.[13]

Along with the phase transitions ferrocene-h_{10} crystal exhibits an interesting disintegration phenomenon at low temperatures. Cooling of single crystals below the λ-type phase transition[14] at 163.9 K leads to crystal disintegration with explosive violence. This phenomenon occurs independently of the λ-type transition in the range 125–108 K depending on cooling rate and/or crystal size.[1,2,15] The strain energy evolved at the disintegration[3] is as large as (1.10 ± 0.11) kJ mol^{-1}, which exceeds even the enthalpy of the λ-type transition. Apart from ferrocene-h_{10}, this kind of phenomenon has not been found for other substances. In this paper we aim to test whether a similar disintegration phenomenon takes place in ferrocene-d_{10} crystal.

Thermodynamic properties of molecular crystals depend primarily on the normal modes of vibration of the lattices and the internal vibrational and rotational degrees of freedom of the molecules. Especially when the constituent molecules are simple, the thermodynamic quantities obtained from calorimetry are satisfactorily compared with those derived from spectroscopic methods. Fortunately, complete assignments of the normal modes have been established for both normal and deuterated ferrocene crystals because ferrocene is a well-studied substance as a representative of sandwich-type compounds. In this respect, comparison of the heat capacities between ferrocene-h_{10} and ferrocene-d_{10} would be quantitatively done.

2. EXPERIMENTAL

Ferrocene-d_{10} was prepared according to the Fritz and Schäfer method.[16] The isotopic purity was determined by the use of high-resolution ^1H NMR of a $CDCl_3$ solution, infrared absorption spectroscopy and elemental analysis after every exchange reaction; the first stage (74%), the second (93%), the third (96.5%) and the final (better than 99.8%). Sieved crystals of grain size 0.84–1.30 mm were used for heat capacity measurements and differential thermal analysis (DTA).

Heat capacity measurements were made between 13 and 300 K with an adiabatic calorimeter.[17] A calorimeter cell[2] contained the specimen of 26.4978 g ($\triangleq$ 0.135125 mol) and a small amount of helium gas to aid heat transfer inside the cell.

The disintegration phenomenon was examined by a DTA-apparatus of our own making. The amount of sample used was about 200–300 mg.

3. RESULTS AND DISCUSSION

Figure 1 represents the DTA curves recorded at a cooling rate of 2.0 K min^{-1} for the sieved crystals of 0.84–1.30 mm. The crystals violently disintegrated into a powder with vast evolution of heat below the λ-point at T_C = 164.1 K. The strain energy evolved at the disintegration was obviously larger than the enthalpy of the λ-type transition. Although the three DTA runs were made for the specimens with

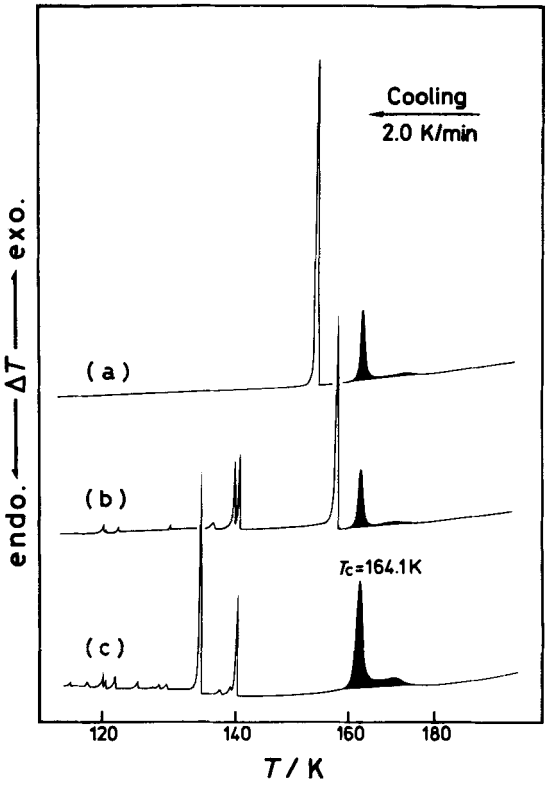

FIGURE 1 DTA curves recorded at a cooling rate of 2.0 K min^{-1} for ferrocene-d_{10} crystals with a sieve fraction of 0.84–1.30 mm. The λ-type transition at 164.1 K and the subsidiary peak at 172 K are shaded in order to distinguish them from the disintegration peaks.

the same sieve fraction, the disintegration behaviors were largely variant: a single-step (Figure 1a) and multi-step disintegrations (Figures 1b and 1c). This fact implies that some unknown factors other than grain size or cooling rate would also govern this phenomenon. At any rate, these features are quite analogous to those of ferrocene-h_{10},[2,3,15] and hence ferrocene-d_{10} is the second example showing the rare disintegration phenomenon.

The results of the calorimetric measurements are listed in Table I. As ferrocene-d_{10} crystal exhibits various phases according to the thermal history of the specimen, each series of measurements is indicated by the relevant phase(s) and the heat treatment done just before the measurement. Figure 2 represents the molar heat capacity at constant pressure, C_p, for all the phases. When the cooling rate was rather high, the high-temperature (HT) phase could easily be undercooled. The specimen thus treated showed a λ-type phase transition centered at T_C = 164.1 K with a secondary C_p maximum at T_{max} = 172 K (solid circles in Figure 2). Around 175 K, however, a gradual temperature drift due to heat evolution was observed. This was caused by the monotropic transition from the undercooled HT phase to the stable low-temperature (LT) phase. Annealing of the specimen at around 190 K for 24 h completed the monotropic transition. The specimen thus obtained showed a first-order transition from the stable LT to the stable HT phase at 251 K (open circles in Figure 2). This phase transition was characterized by a superheating effect of the stable LT phase to about 257 K. The transition temperature of 251 K was determined as the temperature at which the endothermic drift due to the superheating effect ceased after eight days.

The heat capacities of the undercooled HT phase in the range 175–251 K were measured for the specimen rapidly cooled from 300–320 K (series 6, 9–11). Since nucleation of the stable LT phase and its growth proceeded rather slowly at the initial stage, we could obtain several C_p data. When the temperature drift arising from the monotropic transition became large the measurement was terminated. The specimen was heated again to 300–320 K and kept there for 8 h or longer. By repeating this procedure we could determine the C_p values over this temperature region.

It should be noted that, as in the case of ferrocene-h_{10},[1–3] the stable LT phase of ferrocene-d_{10} was realized only through the monotropic transition from the undercooled HT phase around 190 K. Moreover, the extent of this transition depended on both the thermal history and the grain size of the crystal. The monotropic transition was incomplete for the specimen not experiencing the metastable LT phase. However,

TABLE I

Molar heat capacities of ferrocene-d_{10} crystal

T_{av}/K	C_p/J K^{-1} mol^{-1}	T_{av}/K	C_p/J K^{-1} mol^{-1}
Once cooled to 150K, annealed at 190K for 24h		67.589	56.72
		69.908	58.09
		72.278	59.34
Series 1 (stable LT-phase)		74.699	60.64
		77.053	61.93
142.657	100.29	79.350	63.12
144.922	101.80	81.637	64.31
147.230	103.47	83.918	65.47
149.588	105.16	86.202	66.69
151.934	106.95	88.503	67.87
154.278	108.66	90.798	69.08
156.619	110.41	92.092	69.74
158.939	112.14	94.593	71.00
161.246	113.99	97.075	72.38
163.540	115.75	99.559	73.72
165.480	117.26	102.037	74.97
167.072	118.41	104.537	76.38
169.017	120.04	107.048	77.76
171.280	121.98	109.532	79.18
173.504	123.76	112.013	80.59
175.717	125.56	114.524	82.11
178.018	127.34	117.042	83.52
180.488	129.50	119.563	85.07
183.088	131.58	122.105	86.60
185.801	133.81	124.676	88.10
188.556	136.14	127.264	89.71
191.309	138.54	129.838	91.51
193.196	140.00	132.399	93.16
194.532	141.19	134.997	95.01
196.693	143.03	137.579	96.74
199.336	145.27	140.088	98.40
201.953	147.57		
204.553	149.83	Cooled to 10K	
207.144	151.97		
209.669	154.15	Series 3 (stable LT-phase)	
212.122	156.38		
214.618	158.44	13.010	4.82
217.221	160.68	14.011	6.06
		14.848	7.00
Cooled to 53K		15.597	7.82
		16.294	8.67
Series 2 (stable LT-phase)		16.946	9.49
		17.567	10.23
55.655	49.35	18.163	11.02
57.312	50.47	18.745	11.75
59.295	51.76	19.328	12.51
61.226	52.97	19.929	13.34
63.166	54.13	20.599	14.35
65.278	55.35	21.412	15.43

TABLE I *Continued*

T_{av}/K	C_p/J K^{-1} mol^{-1}	T_{av}/K	C_p/J K^{-1} mol^{-1}
22.214	16.48	271.372	203.20
23.014	17.48	274.156	205.25
23.826	18.56	276.922	207.15
24.663	19.60	279.710	209.36
25.333	20.42	282.478	211.39
25.901	21.21	284.716	212.06
26.653	22.19	286.875	213.17
27.645	23.46	288.907	215.27
28.857	24.98	291.944	217.66
30.246	26.68	294.976	219.61
31.815	28.56	298.044	221.87
33.486	30.57	300.944	223.89
35.190	32.31		
36.939	34.05	Rapidly cooled from 303 to 224K	
38.659	35.83		
40.407	37.44	Series 6	
42.410	39.21	(undercooled HT-phase)	
44.605	41.14	225.887	167.74
46.835	42.98	228.507	169.74
49.104	44.75	231.108	171.74
51.419	46.54	233.699	173.69
53.778	48.16	236.287	175.64
		238.876	177.69
Series 4		241.467	179.74
(stable and superheated LT-phases)		244.056	181.72
220.441	163.38	246.648	183.69
223.061	165.55	249.251	185.68
225.654	167.88	251.862	187.71
228.224	170.10		
230.774	172.40	Once heated to 300K	
233.302	174.45	and rapidly cooled to 135K	
236.069	177.16		
238.550	179.44	Series 7	
241.012	181.58	(metastable LT- and undercooled HT-phases)	
243.456	183.65	137.485	102.47
245.883	185.60	140.058	104.79
248.292	187.64	142.583	107.14
250.684	189.62	145.061	109.49
253.060	191.75	147.503	112.05
		149.910	114.67
ΔH (stable LT-phase → stable HT-phase)		152.282	117.56
		154.271	120.11
Series 5		155.835	122.44
(stable HT-phase)		157.381	124.96
255.101	190.57	158.957	128.05
257.732	192.66	160.161	130.88
260.419	194.75	160.855	132.76
263.133	196.65	161.397	135.14
265.841	198.86	161.899	138.42
268.583	201.01	162.360	143.00

TABLE I *Continued*

T_{av}/K	C_p/J K^{-1} mol^{-1}
162.810	151.36
163.242	168.29
163.637	211.86
163.954	355.79
164.212	378.46
164.511	235.92
164.785	186.99
164.993	168.95
165.208	166.73
165.439	163.15
165.833	156.74
166.395	150.71
166.941	147.58
167.464	146.91
168.018	144.69
Annealed at 323K for 133h and rapidly cooled to 105K	
Series 8 (metastable LT-phase)	
107.026	80.42
109.299	81.91
111.635	83.33
114.098	84.89
116.703	86.57
119.356	88.31
122.009	90.18
124.704	92.12
127.404	94.04
130.062	96.13
132.686	98.17
135.275	100.36
Annealed at 190K for 140h	
ΔH (stable LT-phase → stable HT-phase)	
Annealed at 301K for 18h and rapidly cooled to 187K	
Series 9 (undercooled HT-phase)	
188.509	142.56
191.461	144.18
194.368	146.86
200.384	149.90
203.256	151.91
206.132	153.77
209.019	156.59
Annealed at 320K for 8h and rapidly cooled to 168K	
Series 10 (undercooled HT-phase)	
169.444	141.05
170.976	142.42
172.501	142.54
174.049	139.80
175.626	138.18
177.232	137.91
179.202	138.12
181.572	139.10
184.013	140.40
Annealed at 320K for 12th and rapidly cooled to 210K	
Series 11 (undercooled HT-phase)	
211.909	157.59
214.700	159.82
217.491	161.83
220.285	163.92
223.058	165.59
Annealed at 320K for 2h and rapidly cooled to 83K	
Series 12 (metastable LT-phase)	
84.807	68.66
87.515	70.09
90.164	71.48
92.766	72.81
95.333	74.21
97.860	75.60
100.380	76.97
102.896	78.42
105.367	79.83
Cooled to 10K	
Series 13 (metastable LT-phase)	
13.151	7.95
14.016	9.30
14.840	10.40
15.648	11.55
16.458	12.72
17.318	14.16
18.277	15.53
19.313	17.08
20.397	18.64

TABLE I *Continued*

T_{av}/K	C_p/J K^{-1} mol^{-1}	T_{av}/K	C_p/J K^{-1} mol^{-1}
21.536	20.20	52.150	50.66
22.727	22.05	54.209	52.01
23.965	23.76	56.278	53.27
25.236	25.42	58.450	54.57
26.535	27.08	60.720	55.89
27.876	28.67	62.818	57.10
29.297	30.38	64.818	58.19
30.835	32.10	67.020	59.43
32.537	33.92	69.358	60.65
34.308	35.80	71.629	61.83
36.075	37.63	73.816	62.98
37.911	39.38	76.114	64.21
39.853	41.14	78.536	65.39
41.876	42.88	81.015	66.66
43.929	44.80		
45.973	46.21	Annealed at 202K for 48h	
48.016	47.75		
50.071	49.23	ΔH (stable LT-phase → stable HT-phase)	

even if the specimen experienced the metastable LT phase the transition was incomplete when the crystals were initially of powdered form; a few per cent fraction of the undercooled HT phase remained unchanged even after annealing around 190 K for six days. The monotropic transition completed only when the initially large crystals were treated. In this case, the transition finished after annealing for only 24 h. On the other hand, heat treatment at 320 K or higher for longer than 2 h had the sintering effect on powdered crystals. The specimen thus treated behaved just as the initially large crystals.

The λ-type transition at 164.1 K with a subsidiary C_p maximum at 172 K exerts its effect over a wide temperature region from 100 to 230 K. To separate the excess heat capacity from the observed values, a "normal" heat capacity was estimated on the basis of the effective frequency spectrum method[18] by using 125 C_p values in the range 13–100 K and 230–300 K. This method smoothly connected the heat capacities below 100 K and above 230 K, and the 125 C_p values were reproduced within ± 0.44 J K^{-1} mol^{-1}. The enthalpy and entropy of this transition were determined to be $\Delta H = 0.878$ kJ mol^{-1} and $\Delta S = 5.27$ J K^{-1} mol^{-1} by integrating the excess heat capacity with respect to T and ln T, respectively.

In contrast to this, evaluation of ΔH and ΔS for the first-order phase transition at 251 K was straightforward because the transition

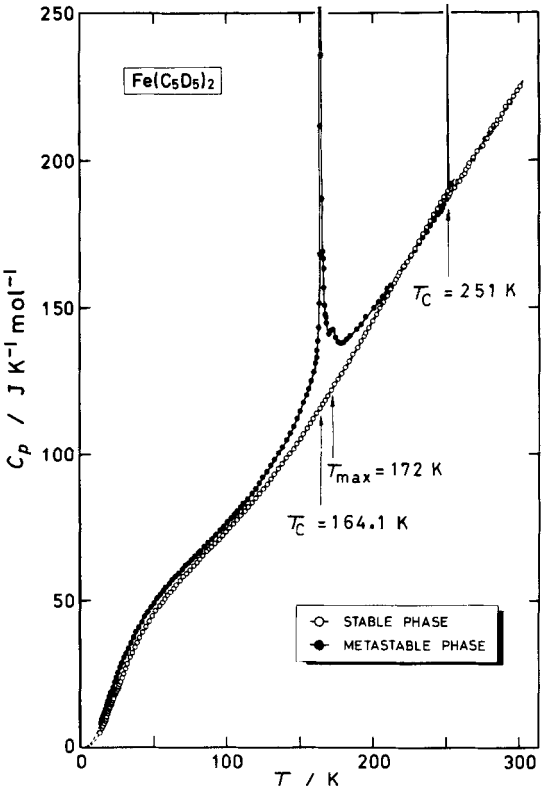

FIGURE 2 Molar heat capacities of ferrocene-d_{10} crystal between 13 and 300 K.

took place isothermally; the corresponding values were $\Delta H = 4.23$ kJ mol^{-1} and $\Delta S = 16.83$ J K^{-1} mol^{-1}.

As shown in Table II, not only the transition temperature but also ΔH and ΔS of the λ-type transition for ferrocene-d_{10} were essentially the same as those for ferrocene-h_{10}. On the other hand, the first-order phase transition exhibited a remarkable isotope effect on the transition temperature by as large a shift as 9 K, whereas the transition entropies were nearly identical. The absence of noticeable isotope effects on the entropies of the λ-type and the first-order transitions suggests that a similar mechanism is responsible for the phase transitions in both substances. The large temperature shift observed for the first-order phase transition implies that the intermolecular interaction relevant to this transition is affected by the mass of the molecule.

In order to correlate various phases of ferrocene-d_{10} in terms of enthalpy and entropy, the heat capacities of the stable and metastable

TABLE II

Data concerning the phase transitions in ferrocene-d_{10} and ferrocene-h_{10} [1,2]

Substance	T_C / K	ΔH / kJ mol^{-1}	ΔS / J K^{-1} mol^{-1}
Ferrocene-d_{10}	164.1	0.878	5.27
Ferrocene-h_{10}	163.9	0.896	5.46
Ferrocene-d_{10}	251	4.23	16.83
Ferrocene-h_{10}	242	4.15	17.13

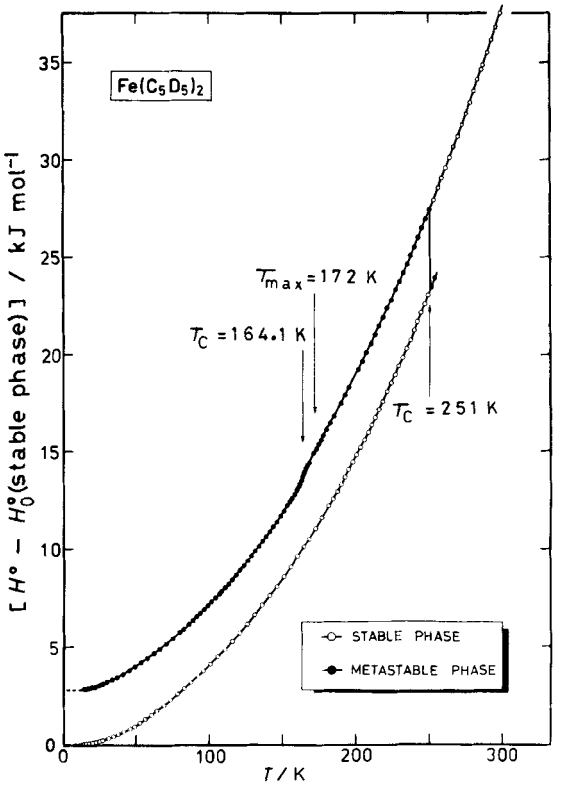

FIGURE 3 Enthalpy relationship among various phases of ferrocene-d_{10} crystal.

LT phases below 13 K were estimated as follows. For the stable LT phase, an effective frequency spectrum was determined by using 132 C_p data in the range 13–251 K. This method reproduced these data within ± 0.25 J K^{-1} mol^{-1}. For the metastable LT phase, the same frequency spectrum as described above was adopted. Figure 3 shows the enthalpy diagram, in which the axis of coordinates indicates the enthalpy increase beyond the zero-point energy of the stable LT phase, [$H°-H_0°$ (stable LT phase)]. The enthalpy of the metastable LT phase at 0 K was found to be by (2.8 ± 0.2) kJ mol^{-1} higher than that of the stable LT phase. This difference is essentially the same as 2.6 kJ mol^{-1} for ferrocene-h_{10}.[1,2]

The entropy diagram is illustrated in Figure 4. If we assume that the stable LT phase obeys the third law of thermodynamics, the entropy of the metastable LT phase at 0 K amounts to (0.38 ± 0.5) J K^{-1} mol^{-1}. This value, though somewhat larger than (0.17 ± 0.5)

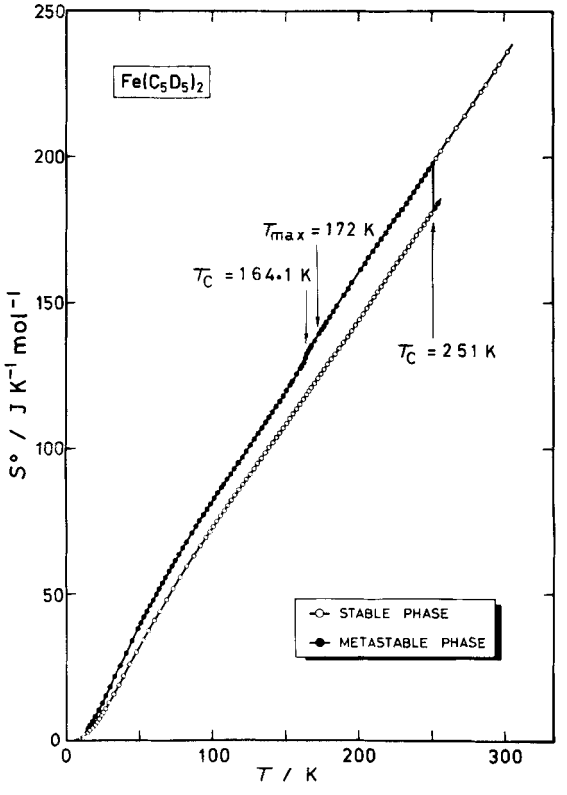

FIGURE 4 Entropy relationship among various phases of ferrocene-d_{10} crystal.

TABLE III

Standard thermodynamic functions for the stable phases of ferrocene-d_{10} crystal (relative molecular mass 196.098)

T / K	C_p° / J K^{-1} mol^{-1}	S° / J K^{-1} mol^{-1}	$(H^\circ - H_0^\circ)/T$ / J K^{-1} mol^{-1}	$-(G^\circ - H_0^\circ)/T$ / J K^{-1} mol^{-1}
10	(2.38)	(0.80)	(0.60)	(0.20)
20	13.45	5.48	4.00	1.49
30	26.37	13.43	9.35	4.08
40	37.06	22.56	15.01	7.55
50	45.44	31.76	20.29	11.48
60	52.20	40.66	25.06	15.61
70	58.14	49.16	29.37	19.79
80	63.46	57.27	33.30	23.98
90	68.66	65.05	36.93	28.11
100	73.94	72.55	40.37	32.18
110	79.44	79.85	43.67	36.18
120	85.33	87.01	46.89	40.12
130	91.61	94.08	50.08	44.00
140	98.34	101.12	53.29	47.83
150	105.47	108.15	56.53	51.62
160	112.99	115.19	59.82	55.37
170	120.88	122.27	63.18	59.10
180	129.07	129.42	66.61	62.80
190	137.40	136.61	70.11	66.50
200	145.85	143.87	73.69	70.19
210	154.45	151.20	77.33	73.87
220	163.01	158.59	81.04	77.55
230	171.70	166.02	84.78	81.24
240	180.70	173.52	88.59	84.93
250	189.06	181.11	92.44	88.67
260	194.42	204.68	112.48	92.21
270	202.12	212.16	115.65	96.51
280	209.57	219.65	118.87	100.77
290	216.13	227.11	122.11	105.00
300	223.24	234.56	125.36	109.20
273.15	204.51	214.52	116.66	97.86
298.15	221.94	233.18	124.76	108.42

J K^{-1} mol^{-1} for ferrocene-h_{10},[1,2] can likewise be regarded as being practically zero within the present experimental errors. This fact suggests that in both the stable and metastable LT phases ferrocene molecules are arranged in regular order though the arrangements are of different kinds. In other words, the metastable LT phase does not belong to a non-equilibrium state. This phase is metastable only in the sense that the Gibbs free energy is higher in this phase than in the stable LT phase.

The standard thermodynamic functions providing numerical values for the phase relationships are summarized in Tables III and IV for the stable and metastable phases, respectively.

TABLE IV

Standard thermodynamic functions for the metastable phases of ferrocene-d_{10} crystal: H_0° means the enthalpy of the stable LT phase at 0 K

T / K	C_p° / J K^{-1} mol^{-1}	S° / J K^{-1} mol^{-1}	$(H^\circ - H_0^\circ)/T$ / J K^{-1} mol^{-1}	$-(G^\circ - H_0^\circ)/T$ / J K^{-1} mol^{-1}
10	(4.13)	(1.45)	(280.84)	(−279.39)
20	18.07	8.38	146.31	−137.93
30	31.16	18.31	105.85	−87.54
40	41.27	28.72	88.50	−59.79
50	49.18	38.82	79.88	−41.07
60	55.47	48.36	75.31	−26.95
70	60.99	57.33	72.88	−15.54
80	66.14	65.82	71.71	−5.90
90	71.39	73.91	71.39	2.52
100	76.77	81.71	71.65	10.05
110	82.34	89.28	72.37	16.91
120	88.77	96.72	73.46	23.25
130	96.08	104.10	74.92	29.19
140	104.73	111.53	76.73	34.80
150	114.78	119.08	78.92	40.17
160	130.50	126.93	81.58	45.35
170	141.55	136.86	86.42	50.44
180	138.45	144.85	89.38	55.47
190	143.38	152.46	92.09	60.38
200	149.71	159.99	94.83	65.15
210	156.93	167.47	97.61	69.86
220	163.70	174.91	100.45	74.46
230	170.89	182.34	103.34	79.00
240	178.58	189.77	106.32	83.46
250	186.26	197.49	109.36	88.13

4. HEAT CAPACITY DIFFERENCE BETWEEN FERROCENE-d_{10} AND -h_{10}

The phase relationship elucidated for ferrocene-d_{10} crystal bears a close resemblance to that of ferrocene-h_{10}.[1,2] Therefore, one may expect that the corresponding phases of the two substances would belong to the same crystallographic system. If this is the case, the crystal structures of the HT, the LT and the metastable LT phases of ferrocene-d_{10} are monoclinic, orthorhombic and triclinic, respectively. This situation makes it favorable to compare directly the heat capacity of ferrocene-d_{10} with that of ferrocene-h_{10}. In addition, the existence of a complete set[19-27] of values for the normal mode frequencies of both the substances makes it possible to calculate the contribution of these degrees of freedom to their heat capacities.

As shown in Figures 5 and 6, apart from the absolute values, shapes of the heat capacity curves of normal and heavy ferrocene crystals

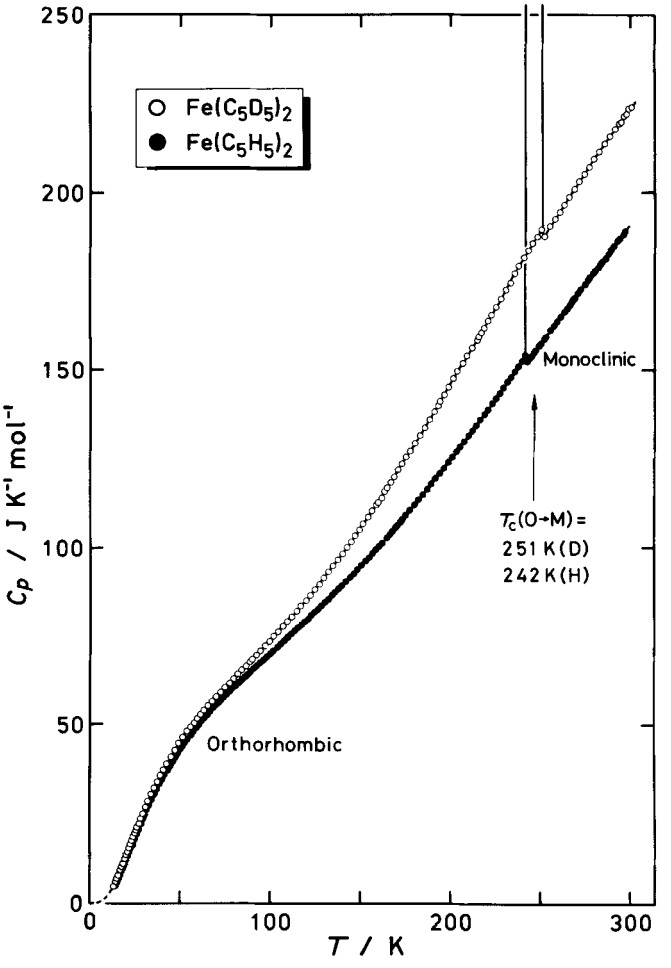

FIGURE 5 Comparison of heat capacity for the stable LT and the stable HT phases between ferrocene-d_{10} and -h_{10} crystal.

resemble each other for all the phases. The heat capacity difference between the two monotonically increases with increasing temperature. To interpret these differences, we analyzed the heat capacity as follows. The heat capacity of a molecular crystal at constant pressure, C_p, consists of three parts:

$$C_p = C_v(\text{lattice}) + C_v(\text{internal}) + (C_p - C_v), \qquad (1)$$

where C_v(lattice) is the heat capacity at constant volume arising from

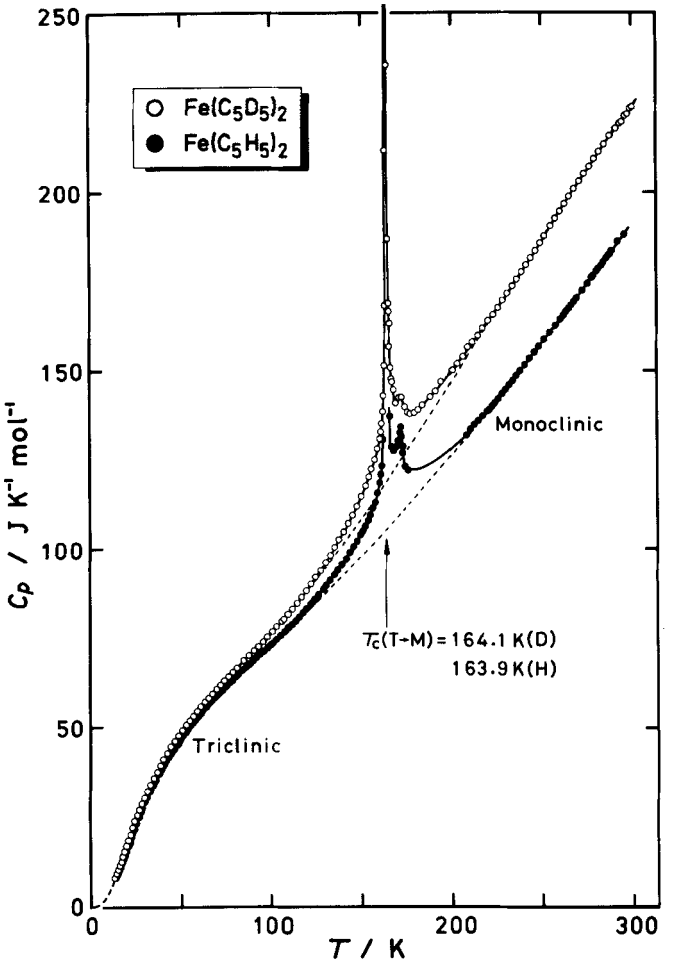

FIGURE 6 Comparison of heat capacity for the metastable LT, the undercooled HT and the stable HT phases between ferrocene-d_{10} and -h_{10} crystal. The broken lines indicate the normal heat capacities separating the excess contribution due to the phase transition from the observed value.

the translational and rotational degrees of freedom of a molecule as a whole, C_v(internal) is the contribution from the internal vibrational and rotational degrees of freedom of a molecule and $(C_p - C_v)$ corresponds to the correction for the expansion work. Since a ferrocene molecule consists of 21 atoms, the total number of the degrees of freedom is 63. Of these, 6 degrees of freedom are relevant to C_v(lattice) while the remaining 57 are connected with C_v(internal). The heat

capacity arising from the internal degrees of freedom is well approximated by the Einstein function, $E(x)$:

$$C_v(\text{internal}) = R\sum_{i=1}^{57} E(x_i),$$

$$E(x) = x^2 e^x/(e^x - 1)^2 \qquad (x_i \equiv h\nu_i/kT), \tag{2}$$

where R, h and k are the gas constant, Planck constant and Boltzmann constant, respectively, while ν_i means the frequency of the ith normal mode. Complete sets[19-27] of ν_i for ferrocene-h_{10} and -d_{10} determined from infrared and Raman spectroscopies are reproduced in Table V for convenience.

Although the orthodox computation of C_v(lattice) should be made on the basis of lattice dynamics, C_v(lattice) is often described by the Debye model in a good approximation. On the other hand, the correction $(C_p - C_v)$ is given by the thermodynamic formula,

$$C_p - C_v = \alpha^2 VT/\beta, \tag{3}$$

where α is the thermal expansion coefficient, V the molar volume and β the isothermal compressibility. In the absence of the data concerning β, the following quasi-thermodynamic relation was used here:

$$C_p - C_v = AC_p^2 T. \tag{4}$$

The constant A and the Debye characteristic temperature θ_D appearing in the Debye model were determined for the respective phases of normal and heavy ferrocene crystals as follows.

According to Eq. 1, the sum of C_v(lattice) and $(C_p - C_v)$ is given as the difference between the observed C_p and the calculated C_v(internal). The averaged values of A and θ_D for 6 degrees of freedom were evaluated by the "best" fit method over the entire temperature region (Figure 7). In this procedure, we treated the metastable LT and the HT phases as an "identical" phase because the change in molar volume at the λ-type phase transition is negligibly small[28] and also because the normal heat capacity curve can smoothly connect these two phases (see Figure 6). As compared in Figure 7, the Debye model including the $(C_p - C_v)$ correction showed fairly good agreement with the experimental values of $[C_p - C_v(\text{internal})]$ for all the phases of ferrocene-h_{10} and -d_{10} crystals. The Debye characteristic temperature was always smaller in ferrocene-d_{10} than in ferrocene-h_{10} crystal. This

TABLE V

Complete sets of values for the normal mode frequencies of ferrocene-h_{10} and -d_{10} crystals[19-27]

Species		Assignment	Wavenumber/cm^{-1} $Fe(C_5H_5)_2$	Wavenumber/cm^{-1} $Fe(C_5D_5)_2$
A_{1g}	1	ν(CH)	3099	2335
	2	δ(CH)	817	619
	3	s. R-breath	1107	1056
	4	s. ν(RM)	313	295
A_{1u}	5	δ(CH)	1254	996
	6	internal rotation	62	52
A_{2g}	7	δ(CH)	1257	998
A_{2u}	8	ν(CH)	3096	2354
	9	δ(CH)	805	635
	10	as. R-breath	1097	1044
	11	as. ν(RM)	474	451
E_{1g}	12	ν(CH)	3085	2318
	13	δ(CH)	998	770
	14	δ(CH)	844	631
	15	s. ν(CC)	1408	1300
	16	s. R-tilt	395	361
E_{1u}	17	ν(CH)	3075	2354
	18	δ(CH)	1003	770
	19	δ(CH)	845	669
	20	as. ν(CC)	1411	1260
	21	as. R-tilt	492	485
	22	δ(RMR)	180	169
E_{2g}	23	ν(CH)	3085	2318
	24	δ(CH)	1191	1053
	25	δ(CH)	1058	855
	26	ν(CC)	1359	1262
	27	R-distortion	882	708
	28	R-distortion	597	526
E_{2u}	29	ν(CH)	3100	2350
	30	δ(CH)	1194	1060
	31	δ(CH)	1048	861
	32	ν(CC)	1345	1260
	33	R-deformation	851	741
	34	R-deformation	569	552

ν: stretching, δ: bending, s.: symmetric, as.: antisymmetric, R: ring, M: metal.

is reasonably accounted for in terms of the mass effect on the lattice vibration. In contrast to this, the coefficient A appearing in the $(C_p - C_v)$ term was larger in ferrocene-d_{10} than in ferrocene-h_{10}. This is caused by the fact that the lattice of the former is soft in comparison with that of the latter and thus larger amplitudes of the lattice vibrations lead to larger expansion of the lattice through the anharmonicity involved in the molecular potential curves.

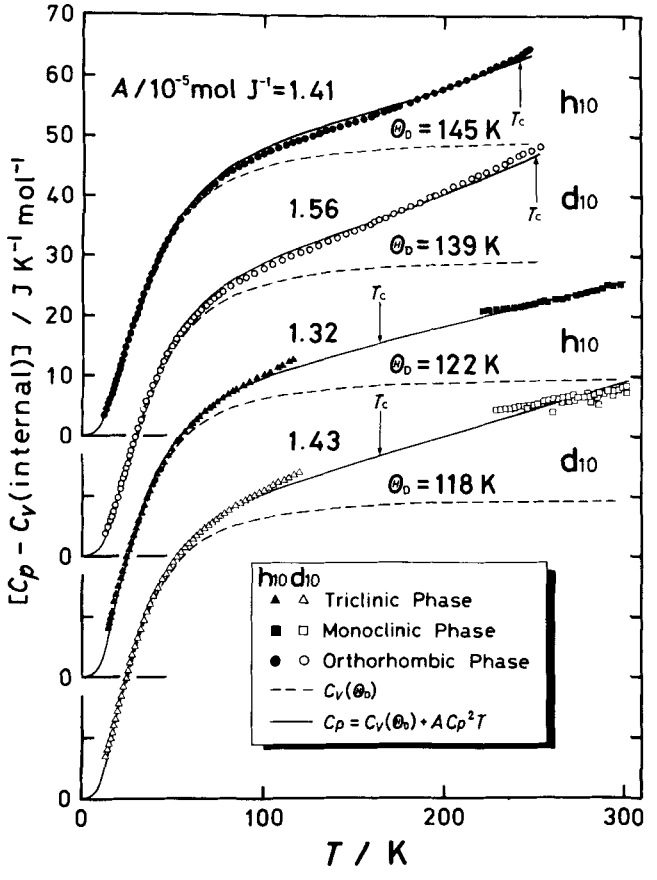

FIGURE 7 Fitness of $[C_p - C_v$ (internal)] with the Debye model including $(C_p - C_v)$ correction for various phases of ferrocene-d_{10} and -h_{10} crystals. The broken lines indicate the Debye model responsible for C_v (lattice) while the solid lines are the sum of C_v (lattice) and $(C_p - C_v)$ correction.

In order to test to what extent the individual terms in Eq. 1 contribute to the heat capacity difference between ferrocene-d_{10} and -h_{10}, we compare the experimental values, $\Delta C_p = [C_p$(ferrocene-d_{10}) − C_p(ferrocene-h_{10})], with the calculated ones in Figure 8. The contribution from C_v(internal) was found to be mainly responsible for ΔC_p. The secondarily large contribution was attributable to the $(C_p - C_v)$ correction, especially at high temperatures above, say, 100 K. In contrast to this, the contribution from C_v(lattice) was important at low temperatures, in particular, below *ca.* 50 K. The sum of these three satisfactorily accounted for the experimental ΔC_p over the whole temperature region.

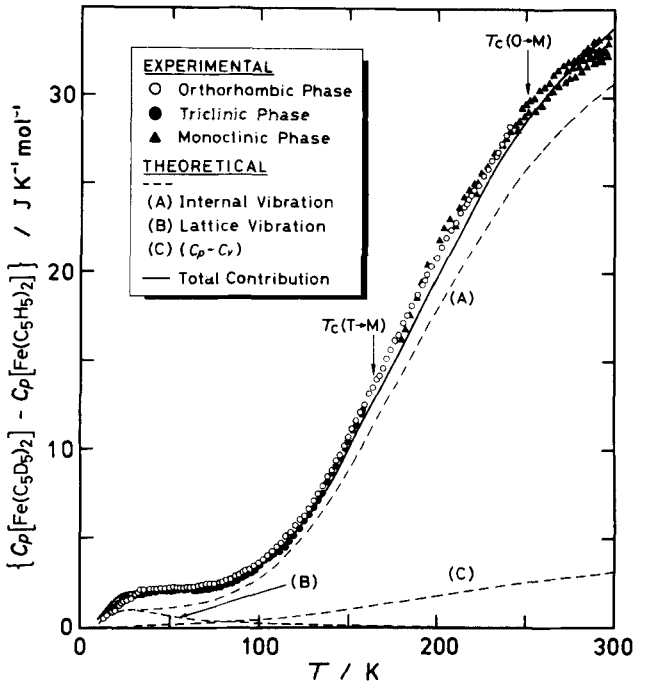

FIGURE 8 The heat capacity difference between ferrocene-d_{10} and -h_{10} crystal for all the phases. The broken lines labelled (A), (B) and (C) are the contributions from C_v (internal), C_v (lattice) and ($C_p - C_v$) correction, respectively. The solid curve is the sum of these three contributions.

Interestingly, the temperature dependence of the experimental ΔC_p for the stable LT phase was identical with that for the metastable LT phase. Moreover, the ΔC_p for the stable LT phase was smoothly connected to that for the HT phase without any discontinuity at the first-order phase transition point. These facts strongly suggest that there exists no structure-sensitive (or phase-sensitive) contribution to the heat capacity difference between ferrocene-d_{10} and -h_{10} crystals.

5. HEAT CAPACITY DIFFERENCE BETWEEN THE METASTABLE AND STABLE LT PHASES

The heat capacity of the metastable LT phase is remarkably higher than that of the stable LT phase even below 100 K where no effect of the λ-type transition is exerted. As in the case of ferrocene-h_{10},[1,2] this fact suggests that the crystal lattice of the latter might be more rigid

than that of the former. In fact, recent X-ray diffraction analysis for ferrocene-h_{10} revealed a large volume change of $\Delta V/V = 0.023$ at the first-order phase transition.[7] Similar change in the molar volume of ferrocene-d_{10} would therefore be expected. In the case of ferrocene-h_{10},[2] the heat capacity difference between the metastable and stable LT phases at low temperatures (below 60 K) was interpreted in terms of a softening of the translational mode along the c-axis from 100 cm^{-1} in the stable LT to 35 cm^{-1} in the metastable LT phase. This model[2] was proposed on the basis of the experimental results obtained from X-ray diffraction[14,28] and Mössbauer effect study[29]; namely, the thermal expansion coefficient of ferrocene-h_{10} along the c-axis is extremely large in the metastable LT phase and anharmonicity of the intermolecular interaction is remarkably large in the c-direction. As shown in Figure 9, this model seems to account for the heat capacity difference between the metastable and the stable LT phase of both ferrocene-h_{10} and -d_{10} crystals.

However, an alternative interpretation seems to be possible. In Figure 10 we compare the experimental value of [C_p(metastable LT phase) − C_p(stable LT phase)] with the difference of [C_v(lattice) + (C_p

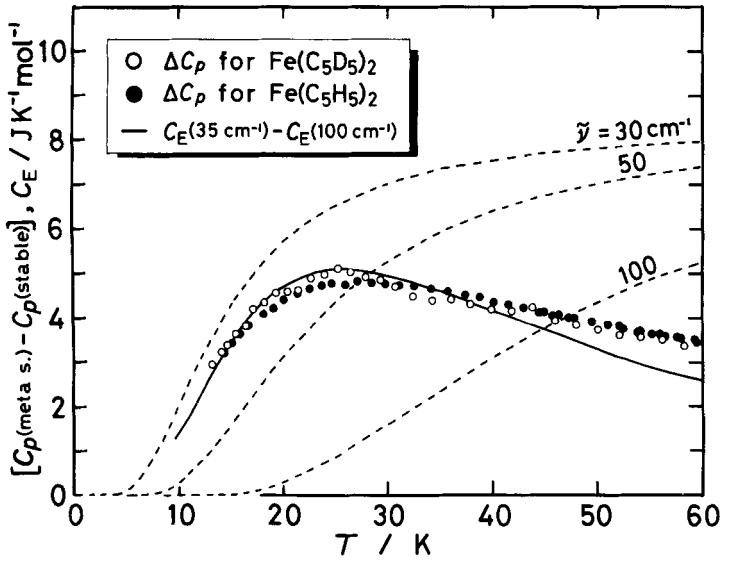

FIGURE 9 Heat capacity difference between the metastable and the stable LT phase, [C_p(metastable) − C_p(stable)], for ferrocene-d_{10} and -h_{10}, and the heat capacity of harmonic oscillators with various wavenumbers, C_E, (broken lines). The solid curve indicates the heat capacity difference between two oscillators with wavenumbers of 35 and 100 cm^{-1}, [C_E (35 cm^{-1}) − C_E (100 cm^{-1})].

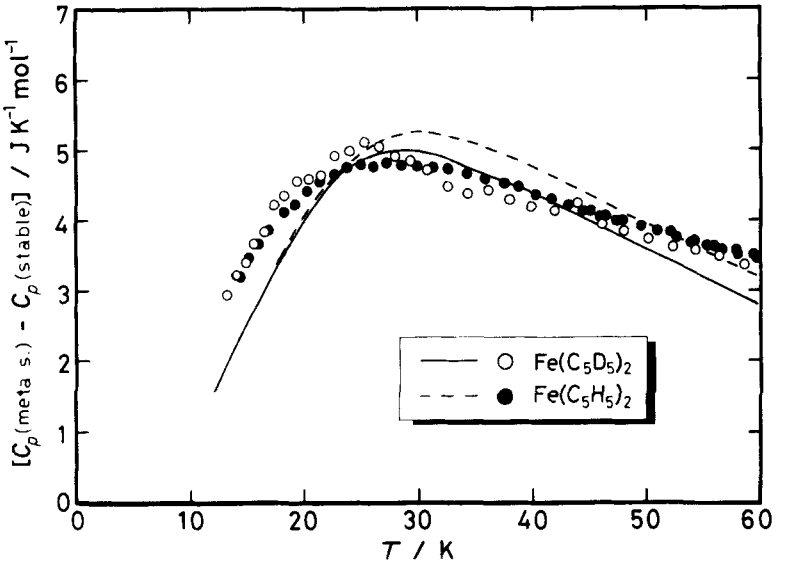

FIGURE 10 Heat capacity difference between the metastable and the stable LT phase, [C_p(metastable) − C_p(stable)], for ferrocene-d_{10} and -h_{10}. The solid and broken lines are the difference of [C_v (lattice) + (C_p − C_v)] between the two phases (*cf.* Figure 7) for ferrocene-d_{10} and -h_{10}, respectively.

− C_v)] between the two phases (*cf.* Figure 7). Since the C_v(internal) is common to both phases, we need not take this term into account. Agreement is not so poor in comparison with the softening model. In other words, the heat capacity difference at low temperatures can be accounted for in terms of either model; one is due to a single mode-softening and the other is an overall-softening of the continuous lattice frequency spectrum. A decision as to which interpretation is reasonable should be deferred until the lattice dynamics of ferrocene-h_{10} and -d_{10} crystals have been studied in more detail.

References

1. K. Ogasahara, M. Sorai and H. Suga, *Chem. Phys. Lett.*, **68**, 457 (1979).
2. K. Ogasahara, M. Sorai and H. Suga, *Mol. Cryst. Liq. Cryst.*, **71**, 189 (1981).
3. M. Naruse, M. Sorai and M. Sakiyama, *Mol. Cryst. Liq. Cryst.*, **101**, 219 (1983).
4. P. Seiler and J. D. Dunitz, *Acta Cryst.*, **B35**, 1068 (1979).
5. F. Takusagawa and T. F. Koetzle, *Acta Cryst.*, **B35**, 1074 (1979).
6. P. Seiler and J. D. Dunitz, *Acta Cryst.*, **B35**, 2020 (1979).
7. J. F. Bérar, G. Calvarin, D. Weigel, K. Chhor and C. Pommier, *J. Chem. Phys.*, **73**, 438 (1980).
8. P. Seiler and J. D. Dunitz, *Acta Cryst.*, **B38**, 1741 (1982).

9. G. Calvarin, G. Clec'h, J. F. Bérar and D. Andre, *J. Phys. Chem. Solids*, **43**, 785 (1982).
10. G. Calvarin, J. F. Bérar and G. Clec'h, *J. Phys. Chem. Solids*, **43** 791 (1982).
11. M. Sorai, S. Murakawa, K. Ogasahara and H. Suga, *Chem. Phys. Lett.*, **76**, 510 (1980).
12. A. Kubo, R. Ikeda and D. Nakamura, *Chem. Lett.*, 1497 (1981).
13. Y. Shiomi and M. Sorai, *Chem. Phys. Lett.*, **95**, 167 (1983).
14. J. W. Edwards, G. L. Kington and R. Mason, *Trans. Faraday Soc.*, **56**, 660 (1960).
15. J. S. Bodenheimer and W. Low, *Phys. Lett.*, **36A**, 253 (1971).
16. H. P. Fritz and L. Schäfer, *Chem. Ber.*, **97**, 1829 (1964).
17. M. Yoshikawa, M. Sorai, H. Suga and S. Seki, *J. Phys. Chem. Solids*, **44**, 311 (1983).
18. M. Sorai and S. Seki, *J. Phys. Soc. Japan*, **32**,382 (1972).
19. E. R. Lippincott and R. D. Nelson, *Spectrochim. Acta*, **10**, 307 (1958).
20. J. Bodenheimer, E. Loewenthal and W. Low, *Chem. Phys. Lett.*, **3**, 715 (1969).
21. R. T. Bailey, *Spectrochim. Acta*, **27A**, 199 (1971).
22. I. J. Hyams, *Chem. Phys. Lett.*, **18**, 399 (1973).
23. I. J. Hyams, *Spectrochim. Acta*, **29A**, 839 (1973).
24. F. Rocquet, L. Berreby and J. P. Marsault, *Spectrochim. Acta*, **29A**, 1101 (1973).
25. J. S. Bodenheimer and W. Low, *Spectrochim. Acta*, **29A**, 1733 (1973).
26. Ya. M. Kimel'fel'd, E. M. Smirnova and V. T. Aleksanyan, *J. Mol. Struct.*, **19**, 329 (1973).
27. K. Yokoyama, S. Kobinata and S. Maeda, *Bull. Chem. Soc. Japan*, **49**, 2182 (1976).
28. G. Calvarin and J. F. Bérar, *J. Appl. Crystallog.*, **8**, 380 (1975).
29. C. R. Hill and P. G. Dibrunner, *J. Phys. (Paris)*, **37**, C6-41 (1976).